Post-prognostics decision-making strategy for load allocation on a stochastically deteriorating multi-stack fuel cell system

Jian Zuo, Catherine Cadet, Zhongliang Li, Christophe Bérenguer, Rachid Outbib

Journal of Risk and Reliability
XX(X):1–30

Post-prognostics decision-making strategy for load allocation on a stochastically deteriorating multi-stack fuel cell system

Jian Zuo[1,2], Catherine Cadet[1], Zhongliang Li[2], Christophe Berenguer[1], Rachid Outbib[2]

Abstract

This work proposes a load allocation decision strategy based on deterioration prognostics information for multi-stack fuel cell systems. The fuel cell deterioration is characterized by the overall resistance value, as it carries the key aging information of a fuel cell. The fuel cell deterioration dynamics is then modeled as an increasing stochastic process whose trend is a function of the fuel cell output power. Combining system deterioration and fuel cell consumption, a multi-objective optimization (MOO) based decision-making strategy is proposed to manage the operation of a multi-stack fuel cell system. Based on this algorithm, the optimal operating power load is computed for each stack. Finally, the performance of the proposed approach is compared to the case without post-prognostics decision for a three-stack fuel cell system. The simulation results show that the proposed post-prognostics decision-making strategy can manage fuel cell system operating in real time by scheduling the optimal load allocation among stacks.

Keywords

Load allocation, Multi-stack fuel cell systems, Multi-objective optimization, Post-prognostics decision-making, Stochastic deterioration, System health management

[1] Univ. Grenoble Alpes, CNRS, Grenoble INP[a], GIPSA-lab, 38000 Grenoble, France
[a] Institute of Engineering Univ. Grenoble Alpes
[2] LIS Laboratory, Aix-Marseille University, 13397 Marseille, France

Corresponding author:
Jian Zuo, Univ. Grenoble Alpes, Grenoble INP, GIPSA-lab, Grenoble Campus, 11 Rue des mathématiques, BP46, Saint Martin D'Heres, Cedex, 38402 Grenoble, France.
Email: jian.zuo@gipsa-lab.grenoble-inp.fr

Introduction

Around the world, actions are taken to fight against climate warming and air pollution. Furthermore, the European "Green Deal"[1] set out a climate change action plan to reduce greenhouse gas emissions by at least 55 % by 2030 to achieve climate neutrality by 2050. To achieve this goal, the wide application of renewable and clean energy is recognized as one of the key solutions. Among solutions, Proton Exchange Membrane (PEM) fuel cell, which uses hydrogen and oxygen as reactant gases and whose only product is water, is regarded as a promising substitute for existing power devices. Nevertheless, the problem of fuel cell durability remains one of the main obstacles to their widespread use[2,3]. To address this challenge, Prognostic and Health Management (PHM) type approaches are proving to be effective[4,5].

PHM is a combination of several processes to monitor, analyze, and diagnose fuel cell State of Health (SoH). The main stages of PHM include: data acquisition and processing, SoH estimation, prognostics, and decision-making. Prognostics is one of the key steps. Based on SoH estimation, the prognostic phase predicts the system's Remaining Useful Life (RUL)[6]. RUL carries vital information about a system and the subsequent decision-making phase relies strongly on it. In summary, PHM deals with three main issues: SoH estimation, RUL prediction, and decision-making strategy[7].

Within these stages, the decision-making process is receiving increasing attention[4]. Indeed, its development requires prior knowledge of the SoH and the RUL of the system under study. In the case of fuel cells, the great complexity of fuel cell operation makes these steps difficult to carry out. This explains why the development of a comprehensive PHM approach for fuel cell systems is challenging.

Fuel cells typically operate in multi-source power generation systems. Consequently, the decision-making strategy consists in deciding the optimal energy distribution between the different devices. Li $et\ al.$[8] proposed an adaptive control strategy to prevent fuel cell from transient and rapid power changes. In Wu $et\ al.$[9], energy distribution is performed by solving a convex optimization problem minimizing the overall energy costs of a hydrogen vehicle. However, the degradation of energy sources tends to be neglected when designing an energy management strategy although it is very important to consider it[10]. Yue $et\ al.$[11] proposed a health-conscious energy management strategy based on prognostics-enable decision-making for fuel cell hybrid electrical vehicle. The proposed approach focuses on energy distribution based on post-prognostics decision-making strategy.

Currently, the application of multi-stack fuel cell systems has received growing research interest. In fact, multi-stack configuration can help improving fuel cell system operation efficiency, extending system lifetime as well as saving fuel costs[12]. Liu $et\ al.$[13] have emphasized the importance of conducting research work on multi-stack fuel systems. It has been shown in[14] that multi-stack systems offer better performance and reliability than single-stack ones due to higher flexibility. In[15], a multi-stack structure has been integrated into an energy microgrid and the simulation results of the model predictive controller (MPC) proves the advantage of the multi-stack fuel cell configuration. On the other hand, optimal energy management strategies have been developed to minimize fuel consumption in[16,17]. [18] proposed a post-prognostic decision process to manage the energy distribution of a multi-stack system to improve their lifetime.[19] further use this model to build stacks allocation strategy on different application scenarios. However, the estimation of the RUL is based on a deterministic deterioration model which limits the interest of the proposed method, in the sense that it cannot capture all the randomness and variability of the considered deterioration phenomena.

Overall, these research works show that multi-stack systems can improve the durability of fuel cells by appropriately managing the distribution of energy in the system and that the decision process must

be designed to allow optimal control actions. The decision-making strategy for energy distribution in multi-stack systems can be formulated as a multi-factor optimization problem. Thus, Liu $et\ al.$[20] developed a hierarchical multi-objective power management strategy to optimize both fuel cell life and energy consumption. Indeed, since saving fuel consumption and decreasing system deterioration are conflicting objectives, a multi-objective Optimization (MOO) technique is suitable for solving this kind of problem[21,22]. An interest of this technique is that the final decision can change with time: at the beginning, we can choose to minimize mainly fuel consumption, and after some time, the decision can be changed to mitigate deterioration to achieve better performance.

The objective of this work is to improve the fuel cell system lifetime while considering the deterioration and hydrogen consumption. This goal is achieved by building a load allocation-based decision strategy. The main contribution of this work is to propose an original power distribution strategy based on post-prognostics decision linking the control strategy with fuel cell deterioration. This work is the first step to build a post-prognostics decision-making strategy to manage power distribution, fuel consumption, and fuel cell deterioration. To do so, the approach used for describing the behavior of fuel cell deterioration is based on stochastic modeling in order to take into account the uncertain phenomena related to this complex process. More precisely, the load-dependent deterioration behavior is modeled using Gamma stochastic process. The main problem consisting in minimizing both the consumption of hydrogen and the effect of deterioration under the constraint of a load satisfaction is formulated as a multi-objective problem with constraints. In order to solve this problem in a realistic amount of time, a methodology based on artificial intelligence is used. The simulation results, based on the proposed strategy for post-prognostic decision-making, show promising performances, which highlights the relevance of the global approach.

To sum up, the contributions of this work to the issue of multi-stack fuel cell system management are the following:

1. Proposing a load-dependent deterioration model based on Gamma stochastic process for the fuel cell, taking the fuel cell stack overall resistance as a health indicator;
2. Developing an original post-prognostics based power allocation strategy to improve the system lifetime and to reduce the fuel consumption of a multi-stack fuel cell, formulated as a multi-objective optimization problem in a uncertain environment;
3. Proposing an approach based on an evolution algorithm to solve the considered multi-objective optimization problem.

The rest of the paper is organized as follow. The working assumptions and model development are presented first and in a second part, a post-prognostics decision-making approach is proposed to resolve the optimal decisions. Instead of developing a management strategy based on deterministic formula, a stochastic deterioration model of a fuel cell stack is developed based on the proposed health indicator. Finally, the simulation results are discussed. The simulation results prove that the proposed strategy can help to extend the system lifetime by 25%.

Working assumptions and model development

Fuel cell system

Fuel cell deterioration The fuel cell is an electrochemical device that converts hydrogen and oxygen into water heat and electricity through the following chemical reactions:

$$\begin{aligned} &Anode : \mathrm{H_2} \rightarrow 2\mathrm{H^+} + 2\mathrm{e^-} \\ &Cathode : 1/2\mathrm{O_2} + 2\mathrm{H^+} + 2\mathrm{e^-} \rightarrow \mathrm{H_2O} \end{aligned} \tag{1}$$

To characterize fuel cell electrical performance, the polarization curve is one of the most widely used techniques. Theoretically, if the Gibbs free energy generated in the reaction could be converted directly into electricity without any loss, the fuel cell would be an ideal voltage generator. In practice, several irreversible losses lower the output voltage. Crossover, activation, ohmic, and concentration losses are considered as the four major irreversible losses. A typical fuel cell polarization curve is shown as Fig. 1. For low current density, fuel cell voltage drop is dominated by activation losses. Then, at the middle range

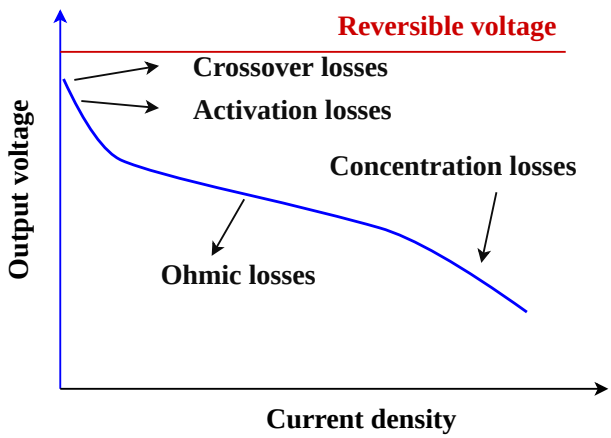

Figure 1. Fuel cell polarization curve with voltage losses.

of current density, the ohmic voltage losses are predominant. And at high current density, concentration losses become dominant. To calculate the fuel cell voltage, a semi-empirical equation derived from the Bulter-Volmer equation and taken from[23] is used:

$$V = n_{cell}\left(E_0 - RI - A\ln(I) - m_1\exp\left(m_2 I\right)\right) \tag{2}$$

where V is the stack voltage, n_{cell} is the number of cells in the stack, I is the fuel cell current density. E_0 is the constant related to reversible potential, A is the Tafel parameter for oxygen reduction, R is the overall resistance, m_1 and m_2 are constant related to the mass transport overpotential. All these parameters can be estimated by fitting this equation to measured fuel cell polarization curves. The power density load of a fuel cell stack L is then calculated through:

$$L = VI \tag{3}$$

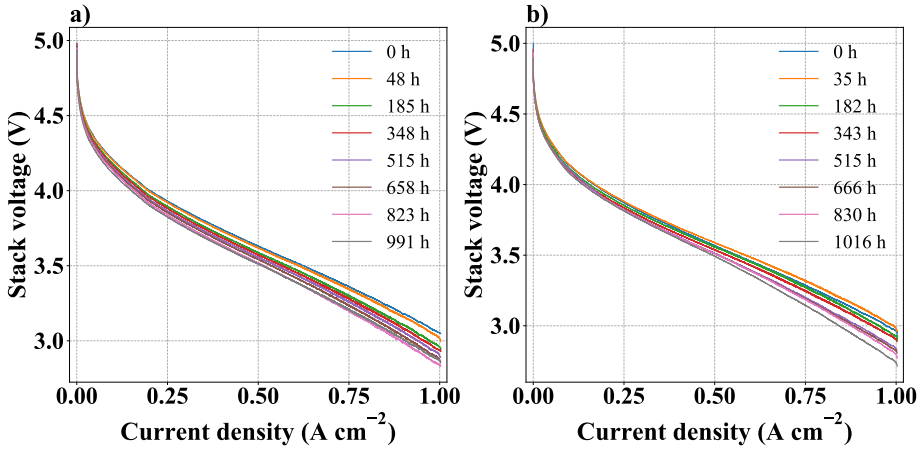

Figure 2. Polarization curves[24] measured for a) Fuel cell stack 1; b) Fuel cell stack 2.

where V is the stack voltage and I is the current density.

The polarization curve is not only representative of the current SoH of the fuel cell, but also reflects its deterioration. This can be seen in Fig. 2, which shows typically measured polarization curves for two tested stacks at different periods taken from the IEEE 2014 data challenge[24]. The fuel cell stack 1 was operated under nominal current load (70 A), and fuel cell stack 2 was operated with a quasi-dynamic condition (nominal current with 7 A oscillations at a frequency of 5 KHz). It can be seen that the output voltage decreases as the fuel cell stacks ages with time.

By fitting the initial polarization curves of the fuel cell of stack 1 at time 0 hour to polarization equation Eq. (2), the initial parameters are calculated and summarized in Table 1. Then the initial electrical performances are further calculated and listed in Table 2.

Table 1. Initial parameters fitting results for Eq. (2).

Parameters	Values
E_0 (V)	0.7971
R_0 ($\Omega\ cm^2$)	0.1803
m_1 (V)	$2.9\times\ 10^{-5}$
m_2 ($cm\ A^{-1}$)	0.009
A (V dec^{-1})	0.0265

Fuel cell health indicator To develop a prognostic approach, a proper health indicator of the fuel cell has to be defined first[25]. This health indicator should be able to reflect fuel cell deterioration state and be easily obtained from measurements. In the work done by Bressel et al.[26], the parameters of the polarization equation (Eq. (2)) have been estimated during all the tested period. The results prove that the overall resistance values of the tested fuel cell are increasing by more than 50% during this

Table 2. Initial electrical performances for fuel cell stack 1.

Operating load level	Min	Nom	Max
Current density ($A\ cm^{-2}$)	0.2	0.7	1
Voltage for one cell (V)	0.8037	0.6803	0.6168
Stack power density (W cm^{-2})	0.8035	2.3811	3.084

experiment. The electrochemical impedance spectroscopy[27] and online estimating algorithms[28,29] ensure that resistance can be measured or estimated.

Hence, the overall fuel cell resistance R can be taken as a global health indicator, and this is the choice we made in this work. However, the degradation is not only driven by time, and the way the fuel cell is operating contributes to make the deterioration rate varying, as shown in[30]. To link fuel cell deterioration with operating conditions, an empirical function is proposed.

To build this function, the nominal power load is considered to lead to the best-operating conditions that deteriorate the least the fuel cells. On the contrary, operating conditions due to lower or higher power load cause higher deterioration rates. Experimental works in[31,32] showed that a high power load will cause irreversible degradation in many parts of the stack, as for example, the electrolyte or the carbon support in the catalyst layer. Similarly,[33,34] proved that a higher deterioration rate is occurring during fuel cell operation at high power load demand. On the other hand, fuel cell damages are even worse when the fuel cell operates at low power[35]. To handle these properties, a parabola deterioration function which represents the different deterioration rates of the fuel cell with respect to power load demand is built (Fig. 3). As can be seen in this figure, the three typical operating conditions are directly depicted. The minimal power, for which the deterioration rate is the highest, the nominal power, which presents the lowest deterioration rate, and the maximal power for which the deterioration rate is high but less than the minimal power. The deterioration rate function, denoted as $D(L)$, is thus expressed as a function of the operating power density L.

Fuel consumption rate Fuel consumption of a fuel cell system is also an important issue from an economic point of view. This consumption is directly linked to the operation of the fuel cell, and more precisely to its operating power. According to the chemical reactions (Eq. 1), the amounts of hydrogen and oxygen consumed by the fuel cell are described as a function of operating current. The expression of the required hydrogen consumption rate f_{H_2} with respect to the stack current can be qualified by Faraday's law[36]:

$$f_{H_2} = \frac{n_{cell} \cdot M_{H_2}}{z \cdot F} \cdot I_{stack} \cdot \lambda \tag{4}$$

where I_{stack}, M_{H_2}, z are stack current in A, molar mass of hydrogen, and number of electrons acting in the reaction (Eq. (1)), respectively. F is the Faraday's constant with a unit of $C\ mol^{-1}$. λ stands for hydrogen excess ratio.

Thus, the hydrogen consumption rate is proportional to the stack current. Besides, hydrogen consumption is also caused by the auxiliary components in fuel cell systems, such as air compressor, humidifiers for example. Several experimental or simulation-based research works proved that a quadratic polynomial equation can be applied to represent the hydrogen consumption rate with respect to the operating power[16,17,37]. Based on these works, the hydrogen consumption rate of a fuel cell stack is

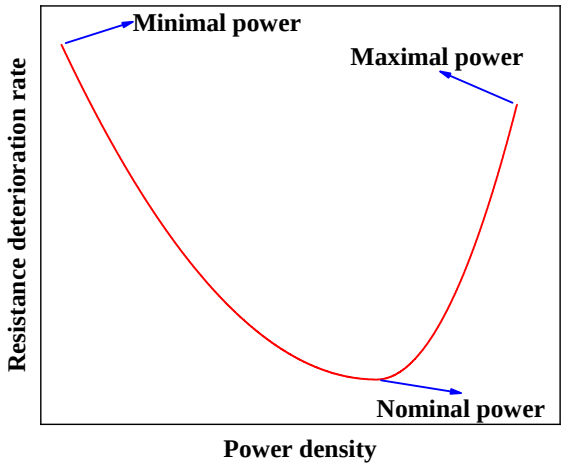

Figure 3. Dependence of fuel cell deterioration rate (overall resistance) on power load demand

expressed as follows:

$$f_{H_2}(L) = aL^2 + bL + c \tag{5}$$

where L is the power density load of a fuel cell, a, b, c are parameters to be fitted.

Deterioration and failure behavior modeling

Deterioration modeling The random evolution of the resistance R as the fuel cell deteriorates is modeled by a Gamma process. A Gamma process is a stochastic process with independent, positive increments (on disjoint time intervals) that obeys a Gamma distribution. As reported in[38], the Gamma process is capable of describing gradual deterioration monotonically accumulating over time. Since the fuel cell resistance deterioration with time corresponds to a monotonic increasing process, and since there is some uncertainty in the aging process, the Gamma process is a relevant tool to model the fuel cell resistance aging phenomenon.

Accordingly, the fuel cell resistance R is modeled by a Gamma process with shape parameter α and scale parameter β, i.e. by definition, the resistance increment $\Delta R(t_1, t_2) \triangleq R(t_2) - R(t_1)$ between time t_1 and t_2 ($t_2 > t_1$) is given by:

$$\Delta R(t_1, t_2) \sim \text{Ga}((\alpha(t_2) - \alpha(t_1)), \beta) \; \forall t_2 > t_1 \geqslant 0 \tag{6}$$

where $\text{Ga}(\alpha, \beta)$ represents the probability density function of the Gamma law with shape parameter α and scale parameter β. The scale parameter β is assigned with a constant value. In this work, only stationary Gamma processes are considered, whose shape and scale parameters do not vary with time (under a constant load), i.e. $\alpha(t_2) - \alpha(t_1) = \alpha(t_2 - t_1)$

On a unit time interval $\Delta t = 1$ h, the mean and variance of the resistance increment ΔR are given by:

$$\begin{array}{ll} \text{Mean}(\Delta R) & = \alpha \cdot \beta \cdot \Delta t \;\; = \alpha\beta \\ \text{Var}(\Delta R) & = \alpha \cdot \beta^2 \cdot \Delta t = \alpha\beta^2 \end{array} \tag{7}$$

In this work, in order to make the degradation load-dependent, the shape parameter α is modeled as a function of the load L. The mean of the resistance increment over a time unit interval, which is also the average deterioration rate (denoted $D(L)$), can thus be expressed as a function of the fuel cell output power L:

$$D(L) = \alpha(L)\beta \tag{8}$$

First hitting-time failure modeling A fuel cell stack is said to fail when the defined health indicator $R(t)$ exceeds a fixed threshold, which is called the failure threshold FT, considered as given. The failure time corresponds to the first hitting-time of level FT by the stochastic process $R(t)$, and it defines the fuel cell stack lifetime denoted T_R, which writes:

$$T_R = \min_t(R(t) > FT) \tag{9}$$

Assuming that the initial resistance R_0 and the failure threshold FT are known for the studied stack, the lifetime distribution can then be written as:

$$\begin{aligned} F(t) = P\left(T_R \leq t\right) &= P\left(R(t) > FT\right) \\ &= \frac{\Gamma\left(\alpha(L)\cdot t, (FT - R_0)\cdot\beta\right)}{\Gamma(\alpha(L)\cdot t)} \end{aligned} \tag{10}$$

where $\Gamma(a,x)$=$\int_x^\infty z^{a-1}e^{-z}\,dz$ is the incomplete Gamma function for $x \geq 0$ and $a > 0$. This work applies P to denote the cumulative probability.

Since the actual aging of the fuel cell depends on the operating conditions, the residual life, i.e. the difference between the expected life and the actual age, needs to be updated regularly. This can be carried out by using the measured resistance value R_{obs} at time t_{obs}, indicator of the actual deterioration level of the fuel cell. Therefore a conditional failure probability $P_d(t)$ at time t after t_{obs} can be defined as the probability for $R(t)$ to exceed a predefined failure threshold before time t, given an observed level R_{obs} at t_{obs}. Thus, based on the previous equation Eq. (10), $P_d(t)$ is written as follows[38]:

$$\begin{aligned} P_d(t) &= F\left(t|R_{obs}(t_{obs})\right) \\ &= P\left(T_R \leq t|R_{obs}(t_{obs})\right) \\ &= P\left(R(t) > FT|R_{obs}(t_{obs})\right) \\ &= \frac{\Gamma\left(\alpha(L)\cdot(t-t_{obs}), (FT - R_{obs}(t_{obs}))\,\beta\right)}{\Gamma\left(\alpha(L)\cdot(t-t_{obs})\right)} \end{aligned} \tag{11}$$

where T_R is the first hitting-time of level FT, L is fuel cell operating power load, $\alpha(L)$ is the corresponding shape parameter and R_{obs} represents the observed resistance deterioration value at the current time step. This conditional failure probability expression will be used at the post-prognostic decision stage in order to integrate the prognostics of the deterioration evolution in the load allocation decision process.

Post-prognostics decision-making

The proposed post-prognostics decision-making strategy for the load allocation for a n-stack fuel cell system is sketched in Fig. 4.

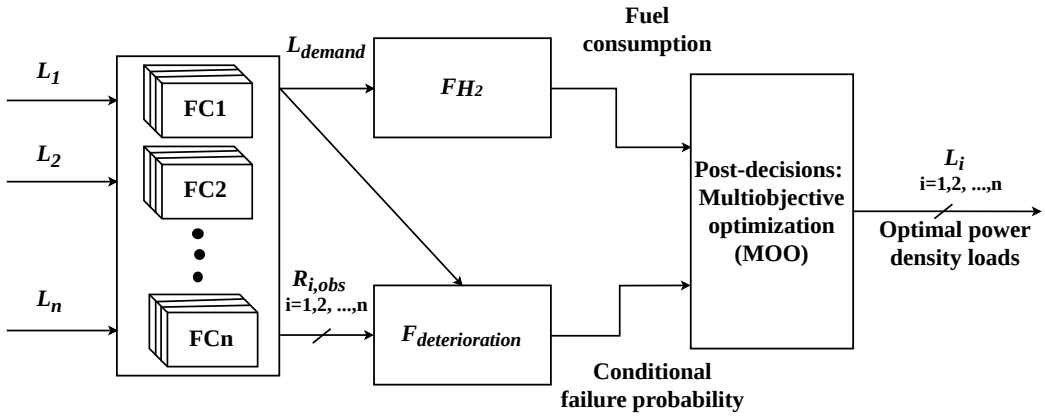

Figure 4. Proposed post-prognostics decision-making strategy for a multi-stack fuel cell system.

A periodical (with period τ) decision-making strategy is considered, under the following assumptions for the multi-stack fuel cell system:

- The fuel cell stacks are physically connected in parallel, but are in series from the reliability point of view, i.e. the system is considered as failed as soon as one stack is failed;
- The fuel cell stacks in the network system are identical, and the output power density of each stack ranges from the minimal output power density L_{min} to the maximum output power density L_{max};
- The values of the fuel cell overall resistances are considered to be measurable whenever necessary, in the sense that a monitoring system and algorithm (e.g. a Kalman filter[26,39]) are assumed to be available to deliver the estimated values of the resistances.

The following sub-sections describe in detail the different features of the load allocation decision-making strategy.

Decision-making principle and policy structure

In order to decide and to adapt the load dynamically to the state of health of the different stacks, a sequential decision policy is carried out. A periodic policy in which the decision is made every time interval of τ hours is considered. At each periodic decision time $k\tau$, the information on the deterioration level, i.e. the overall resistance of each stack is assumed to be available, and the power load allocation is made according both to the deterioration of each stack and to the overall fuel consumption of the multi-stack system.

At each decision time $k\tau$, based on the measured resistance level for each stack $R_{i,obs}^{(k)}$, the conditional probability $P_{i,d}^{(k)}(L_i)$ for this stack to reach a given deterioration level threshold $DT^{(k)}$ at the end of the next period, under a given load L_i), is computed as (similar to Eq. (11), see also Fig. 5):

$$\begin{aligned} P_{i,d}^{(k)}(L_i) &= P\left(T_{DT^{(k)}} \leq (k+1)\tau \middle| R_{i,obs}^{(k)}\right) \\ &= P\left(R_i(k\tau) > DT^{(k)} \middle| R_{i,obs}^{(k)}\right) \\ &= \frac{\Gamma\left(\alpha(L_i)\tau, \left(DT^{(k)} - R_{i,obs}^{(k)}\right) \cdot \beta\right)}{\Gamma(\alpha(L_i)\tau)} \end{aligned} \tag{12}$$

Note that DT in Eq. (12) is not a failure threshold for the stack (contrary to Eq.(11)), but rather a decision threshold used in the decision-making procedure to assess the future deterioration evolution of the considered stack under a given power load L_i, based on its actual deterioration level at the decision time $k\tau$. In order to follow the deterioration evolution of the stack, the value of this decision threshold DT is updated at each decision time step, using the following empirical updating formula:

$$DT^{(k)} = max\left(R_{1,obs}^{(k)}, R_{2,obs}^{(k)}, \cdots, R_{n,obs}^{(k)}\right) + \alpha\beta\tau \tag{13}$$

with α is taken in minimal conditions:

$$\alpha = \alpha(L_{min})$$

Using this heuristic formula, the threshold DT is computed as the sum of the maximum of the current deterioration values and the average deterioration increment over the next period (for the more degrading power load, here L_{min}), which guarantees a value for DT allowing a sensible comparison of the quantities $P_{i,d}^{(k)}(L_i)$.

The decision variables for this decision-making policy are the loads allocated at each stack $L_1, L_2, \cdots, L_n$, adapted at each decision period. We now have to build the objective functions to optimize these decision variables. Based on these deterioration measurements $R_{i,obs}^{(k)}$ and on the estimated $P_{i,d}^{(k)}(L_i)$, two objective functions, function of the decision variables L_i, are evaluated and eventually optimized:

- The first $F_{deterioration}$ is related to the objective of controlling the deterioration by a proper choice of the load allocation among the stacks;
- The second one F_{H_2} corresponds to the objective of controlling the fuel consumption.

At each decision time $k\tau$, the load allocation $\{L_i\}_{i=1,\cdots,n}$ is decided by the optimization of these two objective functions that are detailed in the following sub-section. The periodic decision process is repeated until the system failure. Recall that the multi-stack system is said to be failed as soon as one of the stacks failed (or several stacks failed at the same time). In other words, if the greatest resistance of the system stacks exceeds the failure threshold FT, the whole system failed, which can be written as:

$$max(R_{1,obs}^{(k)}, R_{2,obs}^{(k)}, \cdots, R_{n,obs}^{(k)}) > FT \tag{14}$$

MOO objective function formulation

At each decision time $k\tau$, the problem is stated as a multi-objective optimization problem which consists of the simultaneous optimization of several objective functions, subject to several constraints

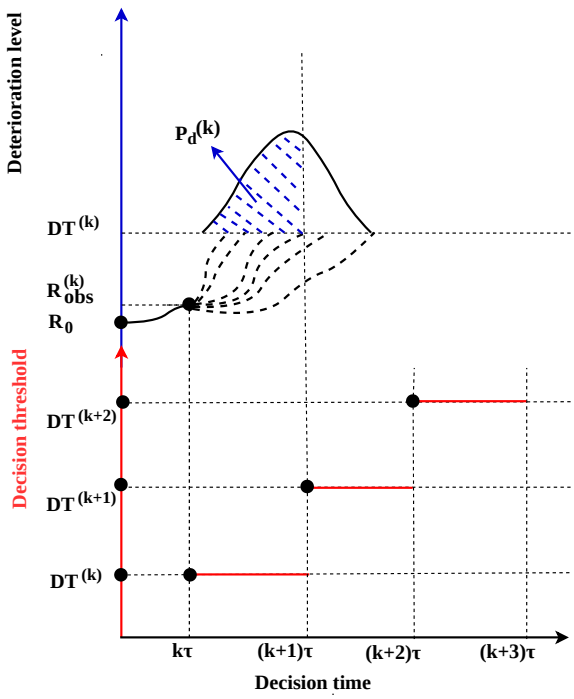

Figure 5. Principle of the determination of the conditional probability distribution for the decision threshold hitting time at each decision time

that determine the feasible set of solutions. Ultimately, the goal is to find a solution on which the decision can evolve with time, as for instance to give priority to one objective function and after some time to give priority to another objective function.

In this work, the objective is to design a decision-making strategy to minimize the life-cycle operation cost of the multi-stack fuel cell system, by acting on two cost key drivers, i.e. prolonging its lifetime (or reducing its degradation) and minimizing its fuel consumption. Two criteria are thus jointly considered - fuel consumption minimization and resistance deterioration minimization -, and the MOO problem consists of two conflict objective functions, namely, $F_{deterioration}$ and F_{H_2}. At each decision time, the two objective functions are evaluated for all the combinations of load allocation that are explored by the optimization algorithm and that fits the power load demand (L_{demand}).The fuel cell system deterioration objective function $F_{deterioration}$ is calculated so as to avoid high failure probability and high deterioration level altogether. Additionally, as shown in a previous work[40], it is interesting to maintain the deterioration trajectories grouped so as to avoid early failures. The multi-optimization algorithm returns a set of non-dominated solutions, and the power load allocation to be applied is chosen thanks to a weighted scalarizing function. Thus, one of the objective functions, that is consumption or deterioration, can be favoured over the other.

Thus, the MOO problem of an n-stack fuel cell system can be formulated as:

$$\begin{aligned} \text{minimize} \quad & (F_{deterioration}, F_{H_2}) \\ \text{subject to} \quad & \sum_{i=1}^{n} L_i \geq L_{demand} \\ & L_{\min} \leq L_i \leq L_{\max}, (i = 1, \cdots, n) \end{aligned} \tag{15}$$

where L_{demand} is the system power load demand, L_{min} and L_{max} are fuel cell stack minimal and maximal output power density loads.

According to Eq. (5), the overall system fuel consumption F_{H_2} is a function of the considered load allocation $\{L_i\}_{i=1,\cdots,n}$ (i.e., the policy decision variables) and is calculated by:

$$F_{H_2} = \sum_{i=1}^{n} \int f_{H_2}(L_i)\, dt \tag{16}$$

The fuel cell system deterioration objective function $F_{deterioration}$ is formulated as a weighted sum of two terms. The first term is a weighted summation of the conditional probabilities $P_{i,d}(L_i)$, see Eq. (12). The weights are given by the ratio of the resistance deterioration $R_{i,obs}$ on the total resistance, which allows to put a strong weight to the stacks that have a high deterioration level, and thus avoid failure as much as possible. The second term is the variance of the resistance deterioration levels, so as to avoid early failure of a stack that would deteriorates much faster than the others. The fuel cell system deterioration objective function $F_{deterioration}$ is a function of the considered load power allocation $\{L_i\}_{i=1,\cdots,n}$ (i.e. the policy decision variables) and of the measured resistance levels $\{R_{i,obs}\}_{i=1,\cdots,n}$ (i.e. the deterioration monitoring information) and it is expressed as:

$$\begin{aligned} F_{deterioration} = \omega_1 & \frac{\sum_{i=1}^{n} (R_{i,obs} \cdot P_{i,d}(L_i))}{\sum_{i=1}^{n} R_{i,obs}} \\ & + \omega_2 \sqrt{\frac{1}{n-1} \sum_{i=1}^{n} \left(R_{i,est} - \bar{R}_{\text{est}}\right)^2} \end{aligned} \tag{17}$$

where $R_{i,obs}$ represents the measured resistance deterioration level for the fuel cell stack i, the corresponding conditional probability is denoted as $P_{i,d}(L_i)$. ω_1 accounts for the weight of fuel cell failure probability, ω_2 determines the weight of variance of the expected deterioration levels of the different stacks. $R_{i,est}$ is the expected deterioration at next decision time step $(k+1)\tau$:

$$R_{i,est} = R_{i,obs} + \alpha(L_i)\beta \cdot \tau \tag{18}$$

The average expected deterioration for n stacks is:

$$\bar{R}_{\text{est}} = \frac{1}{n} \sum_{i=1}^{n} R_{i,est} \tag{19}$$

Now that the objective functions of the defined MOO problem are defined, the next step is to search for a resolution algorithm to solve the optimization problem.

Evolution algorithm-based MOO

To solve the multi-objective problem defined in Eq. (15), a traditional optimization approach, in which a single objective is optimized subject to a given set of constraints, might not be the most appropriate choice. Instead of finding a solution that optimizes all the objectives at the same time, a Pareto optimal set of solutions can be established, in which an improvement of one objective leads to a deterioration in at least one of the others. The framework of MOO allows handling the trade-off among several conflicting objectives, even with different units. One of the most popular Pareto-based EMO algorithms, a non-dominated sorting-based multi-objective evolution algorithm (MOEA) called non-dominated sorting genetic algorithm (NSGA-II), has been successfully applied to many real-life multi-objective optimization problems[41]. The detailed calculation steps of the NSGA-II algorithm are given in Appendix Calculation steps of NSGA-II algorithm and its convergence is studied in Appendix Convergence of NSGA-II algorithm.

An achievement scalarizing function (ASF) based decomposition method is used to choose the final optimal decision within the obtained Pareto Front[42]. According to the principle of ASF, the minimum ASF values calculated from all solutions are chosen as the final optimal decision. The final implementation of ASF-based decision-making is based on the pymoo library[43]. The ASF function is defined by[44]:

$$ASF(f(x), \Omega, \hat{z}^*) = \max_{j=1}^{M=2} \frac{f_j(x) - \hat{z_j}^*}{\Omega_j} \tag{20}$$

where j is either 1 (for $F_{deterioration}$) or 2 (for F_{H_2}); $f(x)$ is the objective function values; $\hat{z_j}^*$ stands for the utopia ("ideal") point of objective j and Ω_j is the assigned (by the user) weight factor for objective j.

Fig. 6 shows the Pareto front, i.e. a set of non-dominated solutions is obtained thanks to the NSGA-II algorithm. The values have been normalized between 0 and 1 for two objective functions, $F_{deterioration}$ and F_{H_2}. Finally, the ASF function-based decomposition approach is applied to find the final optimal decision with respect to defined ASF weights Ω. The weights Ω are chosen by the user, according to his preferences and priorities, so that the preferred objective function has the smallest weight. For fuel cells, usually the main preference is to prioritize the control of the system deterioration (ie a smaller Ω_1), but two weights vectors representing different preferences among the defined objectives are considered in this study. In Fig. 6, two different weights are shown. For $\Omega = (0.5, 0.5)$, an equal importance of $F_{deterioration}$ and F_{H_2} is applied to perform decision-making process. To improve fuel cell durability, $\Omega = (0.2, 0.8)$ will be preferred.

Post-prognostics decision-making algorithm implementation

The algorithm of the post-prognostics decision-making strategy is presented in Algorithm 1. An internal loop estimates the power load allocation for each stack until the failure threshold is reached for one of the stacks. The sequential decision policy adapts the load dynamically to the state of health of the different stacks.

Algorithm 2 shows the evaluation of multi-objective optimization objective function. All values that are needed to calculate $F_{deterioration}$ and F_{H_2} are presented with their calculation equations. Algorithm 2 is called by Algorithm 1 to solve the optimal load allocation decision.

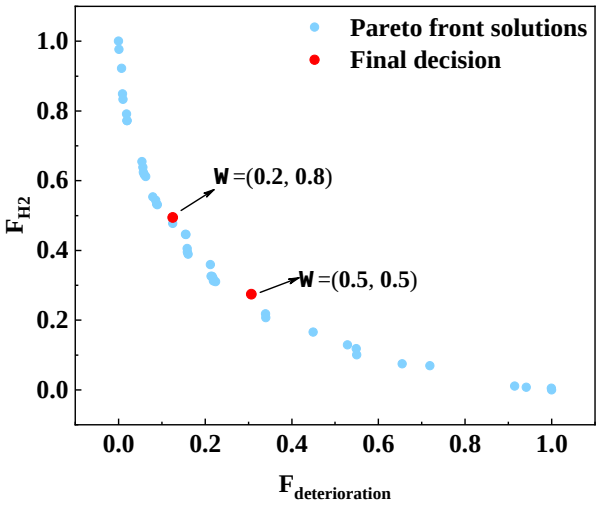

Figure 6. Principle of Pareto front and of final decision-making

Algorithm 1: Main decision-making loop

Data: FT, DT_0, τ, α, β

Initialization $k = 0$, $DT = DT_0$;

repeat

  % At each decision time $k\tau$;

  Measure the resistance deterioration levels $\left(R_{1,obs}^{(k)}, R_{2,obs}^{(k)}, \cdots, R_{n,obs}^{(k)}\right)$;

  Solve the MOO problem through NSGA-II algorithm to return the optimal load allocation $\left(L_1^{(k)}, L_2^{(k)}, \cdots, L_n^{(k)}\right)$;

  % This optimization step include calls to the evaluation procedure of the objective functions (Algorithm 2) to obtain $(F_{deterioration}^{(k)}, F_{H_2}^{(k)})$ *for all the combinations of load allocations that are explored by the optimization algorithm*;

  $k = k + 1$;

  % The system is operated with $\left(L_1^{(k)}, L_2^{(k)}, \cdots, L_n^{(k)}\right)$ *until next decision step*;

until $max\left(R_{1,obs}^{(k)}, R_{2,obs}^{(k)}, \cdots, R_{n,obs}^{(k)}\right) > FT$ *% System failure*;

Performance evaluation

Once the proposed power distribution strategy is implemented, its performance should be evaluated through proper estimation indexes. One performance index is the system lifetime. For a n-stack fuel

Algorithm 2: Evaluation of the objective functions for multi-objective optimization

Input: Measured deterioration levels $\{R_{i,obs}\}_{i=1,\cdots,n}$; Candidate loads per stack $\{L_i\}_{i=1,\cdots,n}$
Output: $F_{deterioration}(\{R_{i,obs}\}_{i=1,\cdots,n}, \{L_i\}_{i=1,\cdots,n})$, $F_{H_2}(\{L_i\}_{i=1,\cdots,n})$

1 Calculate system fuel consumption objective function: $F_{H_2}(\{L_i\}_{i=1,\cdots,n})$ ⟵ Eq. (16);
2 Using $\{R_{i,obs}\}_{i=1,\cdots,n}$, calculate the expected deterioration resistances and the average expected deterioration: $R_{i,est}$ ⟵ Eq. (18), $\bar{R}_{\text{est}}$ ⟵ Eq. (19) ;
3 Update decision threshold DT ⟵ Eq. (13);
4 Using $\{R_{i,obs}\}_{i=1,\cdots,n}$ and $\{L_i\}_{i=1,\cdots,n}$, calculate the conditional probabilities $P_{i,d}(L_i)_{i=1,\cdots,n}$ ⟵ Eq. (12);
5 Calculate system deterioration objective function $F_{deterioration}(\{R_{i,obs}\}_{i=1,\cdots,n}, \{L_i\}_{i=1,\cdots,n})$ ⟵ Eq. (16);
6 Return $(F_{deterioration}, F_{H_2})$

cell system, the system lifetime for one run simulation (EoL) is calculated by:

$$EoL = min(T_{1,R}, T_{2,R}, \cdots, T_{n,R}) \tag{21}$$

where $T_{i,R}$ is the end of lifetime of stack i as defined in Eq. (9). The mean system lifetime ($\overline{EoL}$) can then be estimated by averaging the results over the N-run simulations:

$$\overline{EoL} = \frac{1}{N}\sum_{i=1}^{N}(EoL_i) \tag{22}$$

Additionally, a second performance index with respect to fuel consumption should be proposed. However fuel consumption alone is not suitable, as when the system life is extended, it automatically consumes more fuel. Therefore a ratio representing the operating time per unit quantity of consumed fuel is used. Thus, the greater is the index, the lower is fuel consumption. The mean value of the index is determined with :

$$\overline{Ratio} = \frac{1}{N}\sum_{i=1}^{N}(EoL_i)/F_{H_2,i} \tag{23}$$

where the unit is h kg^{-1}. The same calculation approach is applied for the median system lifetime (EoL_{med}) and Median Ratio ($Ratio_{med}$).

Results and discussion

Simulation conditions

The simulations are performed with a 3-stack fuel cell system. To be as realistic as possible, the simulation parameters have been tuned with real data provided by the IEEE PHM 2014 data challenge, realized with two 5-cell stacks[24].

The simulations are carried out for two constant power load values. Even if in practice the power load is not perfectly constant, we make this assumption considering that the small fluctuations in the demand are handled by using an energy storage buffer and that their effect on the load allocation strategy can be ignored. The first value, $L_{demand} = 7.8$ W cm^{-2} is relatively high and constrains the system to operate with a power greater than the nominal one. A lower value, $L_{demand} = 6.6$ W cm^{-2}, is also investigated in the simulations. This value is relatively low and the fuel cell operates at a power lower than the nominal one.

The value of decision time interval τ has to be neither too big nor too small so that the effect of the control strategy is visible. Therefore, the decision time interval τ is set to 100 h. The value of failure threshold FT is chosen thanks to the experimental dataset, with a lifetime T_R of 1000 h. Therefore, the value of FT is taken as 0.453 Ω cm^2. To estimate the Pareto optimal set of solutions, the NSGA-II algorithm, presented in section Calculation steps of NSGA-II algorithm, is configured with an initial population size of 300, and the number of offspring created through the mating of 160. At each decision step, an optimal set of solutions is determined for the two objective functions $F_{deterioration}$ and F_{H_2}. Then, two final decisions are selected thanks to the weights of the scalarizing function. The first one with both weights of 0.5 to each objective function ($\Omega = (0.5, 0.5)$), means that no objective is preferred, and the other one with a preference for limiting the degradation, so the weight of 0.2 to degradation objective function and thus 0.8 to the fuel consumption objective function ($\Omega = (0.2, 0.8)$).

The results are compared with two well-known existing strategies :

a) The Daisy chain strategy, which distributes the system load demand sequentially to the fuel cell stacks. Here, two fuel cell stacks operate at the nominal power condition, and the third one supplies the remaining power.
b) The Average load strategy, which distributes the overall system load demand evenly among all stacks.

Deterioration parameters fitting

The parameters to calculate of the objectives functions F_{H_2} and $F_{deterioration}$ formulated in Eq. (16) and Eq. (17) are estimated with the IEEE 2014 data challenge data.

On one hand, the calculation of the overall fuel consumption F_{H_2} is based on the fuel consumption rate $f_{H_2}(L)$ (Eq. (5)). The parameters of this polynomial equation are estimated by using non-linear least squares algorithm to fit this function to fuel consumption data. The values are a=0.00023, b=0.001, and c=0.00018.

On the other hand, the calculation of system deterioration $F_{deterioration}$ with Eq. (17) needs the estimation of the $\alpha(L)$ and β parameters for the conditional failure probability P_d calculation and the weights ω_1 and ω_2. First, the $\alpha(L)$ and β parameters are estimated for operation in nominal power. The estimation process is presented in Appendix Gamma process - scale and shape parameters estimation. The estimated values are α_{nom}=0.01125 and β=0.02424. In addition, the expected lifetime for the nominal condition is set as 1000 hours based on the data reported in the IEEE 2014 data challenge.

Then, to estimate the equation of the resistance deterioration rate $D(L)$ with respect to power load (Fig. 3), three points have to be determined for respectively minimal, nominal and maximal power conditions from available data. To that end, we assume that the minimal and maximal expected lifetimes are 400 and 450 hours respectively. Then, the shape parameter range is calculated as α_{min}=0.02805 and

α_{max}=0.02505. Thus, the resistance deterioration rate is calculated as:

$$D(L) = (C \times (L - 2.3811)^2 + 2.727) \times 10^{-4} \tag{24}$$

with

$$C = \begin{cases} 1.6364 & L_{\min} \leq L < L_{nom} \\ 6.77 & L_{nom} \leq L \leq L_{\max} \end{cases}$$

where $D(L)$ represents the deterioration rate of R, L is fuel cell operating power load. L_{min}, L_{nom}, and L_{max} are fuel cell operating power density load for minimal, nominal, and maximal conditions, with their values reported in Table 2.

With the above simulation parameters, the weights introduced in Eq. (17) (section MOO objective function formulation) are investigated based on actual simulation effects. It is proved that $\omega_1 = 12$, and $\omega_2 = 1.2$ can capture fuel cell deterioration well, enable the decision-making strategy to control the system efficiently. Therefore, these values are used in the post-prognostics decision-making strategy.

Table 3 summarizes the key parameter fitting results.

Table 3. Key parameters used in this work.

Parameters	R_0	α_{min}	α_{nom}	α_{max}	β
Values	0.1803	0.0281	0.0113	0.0251	0.0242

Number of simulation runs determination

Due to the randomness of the gamma process, the number of simulation runs must be sufficient to make the results statistically stable. However, a too large number of simulation runs will lead to undue computational cost. Therefore, this number has to be adjusted.

By the law of large numbers, the sequence of simulated average lifetimes converges to the expected value. For each value of power load demand considered, $L = 6.6$ W cm^{-2} and $L = 7.8$ W cm^{-2}, 8000 independent simulations were performed. Based on these runs, an accumulated average system lifetime is calculated. The simulation results show that when the number of simulation runs increased to 1500, the average system lifetime converges to a single value. Therefore, the following simulation results are analyzed based on 1500 independent simulation runs.

Simulation results for $L_{demand} = 7.8$ W cm^{-2}

Fig. 7 presents the detailed one-run simulation results for $L_{demand} = 7.8$ W cm^{-2}. Fig. 7(a) shows the evolution of the overall resistance of each stack and the power load allocation for $\Omega = (0.5, 0.5)$. At time 0 h, the overall resistances of the three stacks are initialized at $R_0 = 0.1803$, and a first post-prognostic decision making is performed, giving the power load allocation $(L_1, L_2, L_3) = (2.6, 2.6, 2.6)$ W cm^{-2} to be applied. After $\tau = 100$ h of operation, another post-prognostics decision is performed. It can be found out that, though the stacks are assumed to be identical and have the same initial deterioration, their states of health vary. FC2 has the highest deterioration level, followed by FC3 and FC1. The optimal power loads calculated by proposed post-prognostics decision-making strategy are $(L_1, L_2, L_3) = (2.695, 2.539, 2.565)$. FC1 is assigned to the highest power density to balance the system

deterioration and fuel consumption. The third post-prognostic decision is performed at 200 hours. FC3 reaches the highest resistance value. Thanks to decision-making control, the deterioration rate of FC2 is much slower compared to the previous decision step. In this case, the measured resistance of FC2 puts a heavy weight on the objective function $F_{deterioration}$ of Eq. (17), so as to avoid FC2 to deteriorate more. Thus, FC3, which had a lower deterioration at the previous decision step, deteriorates is slightly more than FC2. By doing this, the stacks that are more deteriorated can be assigned to a power density load closer to the nominal value, and thus slow down their deterioration. Similar results can be observed for the following decisions. The one-run simulation terminates at 714 h when FC3 reaches FT. From the data in Fig. 7(b), the control effects are more obviously seen. It is observed that it is not always the same fuel cell that is the most deteriorated though the lifetime is shorter in this case. A bigger weight is assigned to control fuel cell deterioration, thereby preventing the most deteriorated fuel cell from further fast deteriorating. This result is consistent with the design of $F_{deterioration}$ as shown in Eq. (17), and the ASF function.

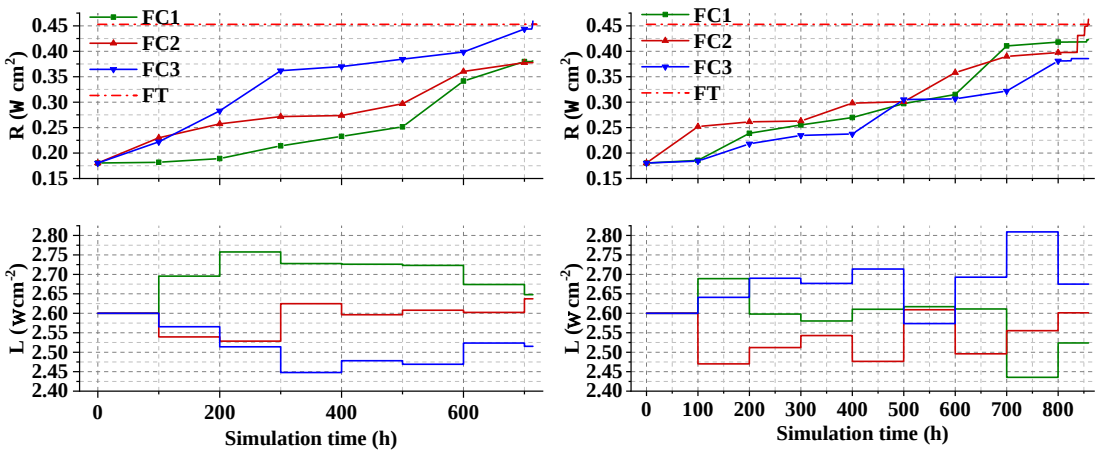

(a) $\Omega = (0.5, 0.5)$ (b) $\Omega = (0.2, 0.8)$

Figure 7. One-run optimal load allocation and system deterioration for $L_{demand} = 7.8$ W cm^{-2}.

Fig. 8 presents histograms of the system lifetime obtained with 1500 runs, for different load allocation strategies. The post-prognostics decision-making with no preference ($\Omega = (0.5, 0.5)$) and with preference for limiting the degradation ($\Omega = (0.2, 0.8)$) are compared with the daisy chain and the average load strategies. The histograms obtained with the post-prognostics decision-making and the average load strategies are mostly distributed in the range (400; 1000) h, whereas the lifetimes for the Daisy chain algorithm are mainly distributed in (300; 900) h. For the Daisy chain, the worst results can be explained by the fact that, as two stacks operate at their nominal power density load, the third one adapts to the power load demand and thus operates with conditions that will damage the stack. In addition, one can see

in this figure that the distribution for the Daisy chain case is more grouped with a peak at 600 h, which is not the case for the other strategies.

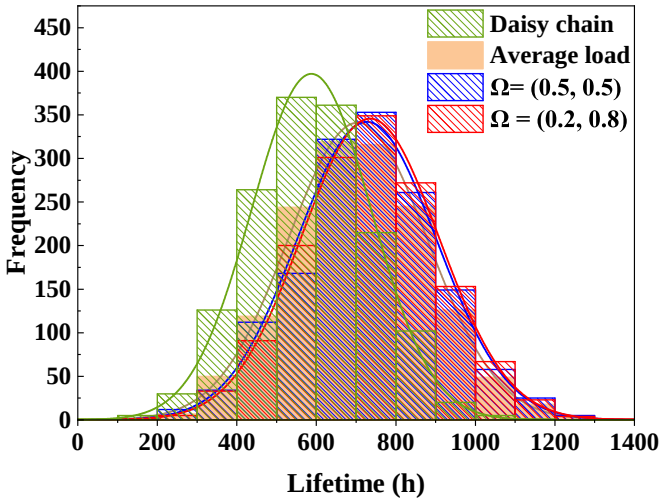

Figure 8. Histograms (and fitted Gaussian pdf) of the system lifetime for $L_{demand} = 7.8$ W cm^{-2}, under different load allocation strategies.

Fig. 9 shows the simulated deterioration trajectories of $\Omega = (0.2, 0.8)$ and of the average load split strategy. 50-run trajectories are plotted among the 1500 simulated trajectories. This figure shows that the trajectories simulated with the proposed decision-making strategy tend to be more grouped together and with a lower variance than the one simulated with the average load split strategy. This is the result that was expected with the second term of Eq. (17), that is the sum of the variance of the resistance deterioration. This helps to avoid situations where one stack in the system deteriorates too fast leading to the failure of the overall system. This effect is also visible in the previous lifetime histogram.

Further results are given in Table 4 which summarizes statistical results for $L_{demand} = 7.8$ W cm^{-2}. In this table, it can be seen that the mean lifetime and the medium lifetime are better for the proposed strategy, and it confirms that the Daisy chain strategy has the worst results. For the proposed strategy, a slight difference can be noticed between the two weights distributions, showing that the $\Omega = (0.2, 0.8)$ allocation leads to a mean lifetime of 735 hours, which is the highest among all simulation cases. The results for the Ratio index, whether it be mean or median, are very close together. The Ratio of the Average load split is the highest, that is the largest operating time per quantity of consumed fuel, with both Mean and Median ratio of 21.3603 h kg^{-1}. Then followed by $\Omega = (0.5, 0.5)$, with Mean and Median ratio of 21.3525 h kg^{-1} and 21.3545 h kg^{-1}. These results show that increasing the fuel cell lifetime does not mean that the fuel consumption is exploding accordingly.

Simulations were also conducted for a relatively lower system demand case, $L_{demand} = 6.6$ W cm^{-2}, to check the control effects of the proposed strategy.

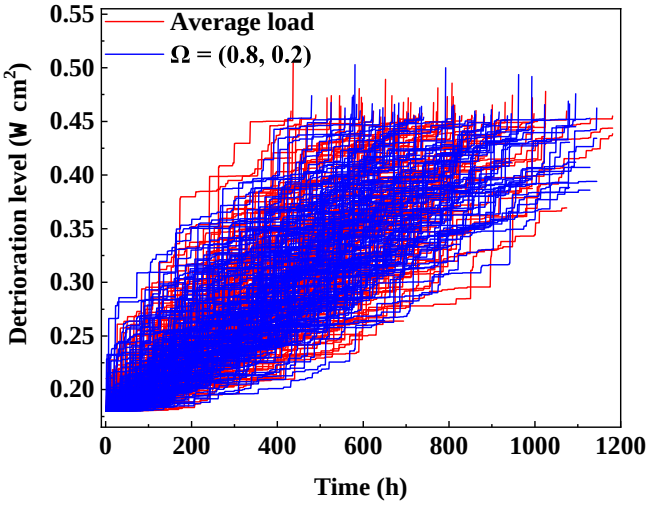

Figure 9. System resistance deterioration trajectories (50-run) for $L_{demand} = 7.8$ W cm^{-2}.

Table 4. 1500 runs simulation statistic results for $L_{demand} = 7.8$ W cm^{-2}.

Simulations	$\overline{EoL}$	EoL_{med}	$\overline{Ratio}$	$Ratio_{med}$
Daisy chain	587	588	21.2522	21.2522
Average load	704	703	21.3603	21.3603
$\Omega = (0.5, 0.5)$	727	727	21.3525	21.3545
$\Omega = (0.2, 0.8)$	735	731	21.3450	21.3501

Simulation results for $L_{demand} = 6.6$ W cm^{-2}

Fig. 10 provides the detailed one-run results for $L_{demand} = 6.6$ W cm^{-2}. Similarly to $L_{demand} = 7.8$ W cm^{-2}, the overall resistances of the stacks are initialized to R_0 at time 0 h. At that time, a post-prognosis decision is carried out, giving the allocation of $(L_1, L_2, L_3) = (2.268, 2.271, 2.269)$ W cm^{-2}. Then at $\tau = 100$ h, a second decision is performed. The most deteriorated fuel cell, FC2, with $R = 0.2746$ Ω cm^2, is assigned to a power load close to the nominal value so as to mitigate its deterioration. The optimal allocation is then $(L_1, L_2, L_3) = (2.218, 2.353, 2.197)$ W cm^{-2}. As shown in Fig. 10(a), FC2 tends to have the highest deterioration during all the operation period. The decision-making strategy lets FC2 operates at a near nominal condition to mitigate its deterioration. While for the stacks with a relatively lower deterioration, the decision-making strategy will assign less desirable operating loads to satisfy the system power demand. However, it can be seen from the deterioration path of FC2 that even though a favorable power is provided, it still deteriorates more rapidly than others because of the randomness. Fig. 10(b) shows the simulation results when the priority is assigned to deterioration mitigation with $\Omega = (0.2, 0.8)$. It is observed that from 0 to 200 h, the deterioration levels of the three stacks are closed to each other. At 300 h, FC3 has the highest deterioration level, followed by FC1 and FC2. However, from 300 to 600 h, the deterioration rate of FC3 is gradually decreasing and tends to be the lowest. And the

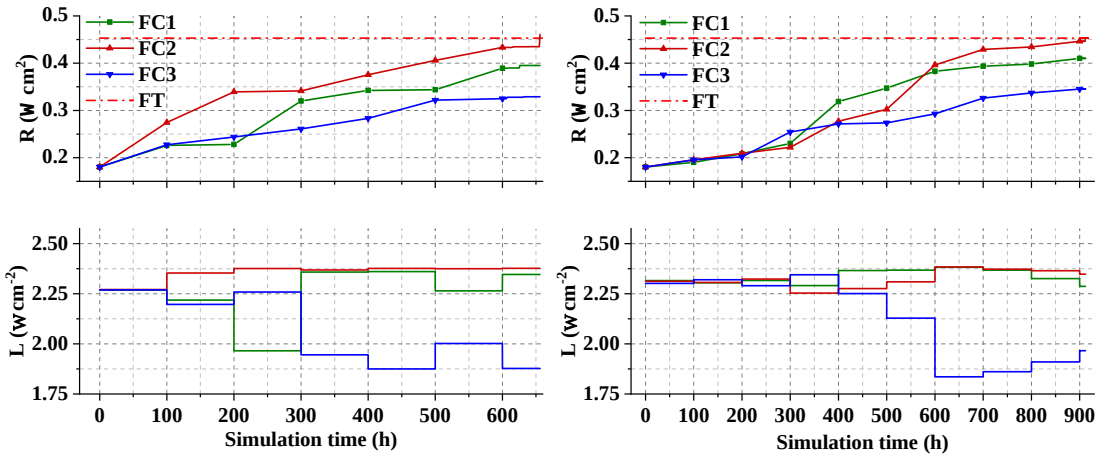

(a) $\Omega = (0.5, 0.5)$ (b) $\Omega = (0.2, 0.8)$

Figure 10. One-run optimal load allocation and system deterioration for $L_{demand} = 6.6$ W cm^{-2}.

deterioration rate of FC2, initially less deteriorated, is increasing. By comparing the results of different Ω values, it is observed that it is not always the same fuel cell that is the most deteriorated though the lifetime is shorter with $\Omega = (0.2, 0.8)$. These results are consistent with those that have been reported in section Simulation results for $L_{demand} = 7.8$ W cm^{-2}.

Fig. 11 shows the histogram of the system lifetime for different strategies both with post-prognostics decision-making or not. This time the histogram allocation of the Daisy chain is similar to the other ones, and the lifetimes are mostly distributed in the range $(400; 1100)$ h. However, the average load split strategy achieves a slightly longer lifetime than the Daisy chain, and the proposed decision-making strategy is even better. Indeed, for $\Omega = (0.2, 0.8)$ and $\Omega = (0.5, 0.5)$, their system lifetimes are more frequently in the range $(800; 1400)$ h than the Daisy chain and average load strategies.

Fig. 12 presents 50-run deterioration trajectories for $\Omega = (0.2, 0.8)$ and average load split strategies. Similar to the results reported in Fig. 9, the deterioration trajectories with decision-making control appear to be more grouped together than the comparison strategy. The statistical results for $L_{demand} = 6.6$ W cm^{-2} are summarized in Table 5. As can be seen, a longer lifetime is achieved for simulations with the decision-making strategy. In addition, the decision strategy that prioritize lifetime with $\Omega = (0.2, 0.8)$ obtains the highest lifetime among the four simulation cases. The Ratio index results are similar to those in section Simulation results for $L_{demand} = 7.8$ W cm^{-2}, with very close values. These results show that the proposed decision-making strategy can be applied in practice to improve fuel cell system lifetime without consuming far more fuel.

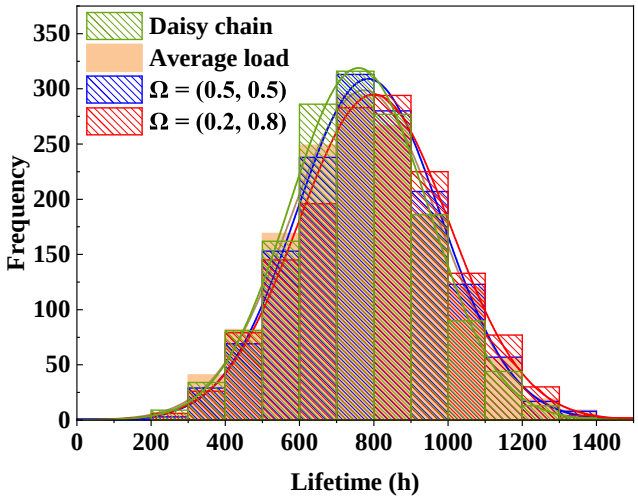

Figure 11. Histograms (and fitted Gaussian pdf) of the system lifetime for $L_{demand} = 6.6$ W cm^{-2}, under different load allocation strategies.

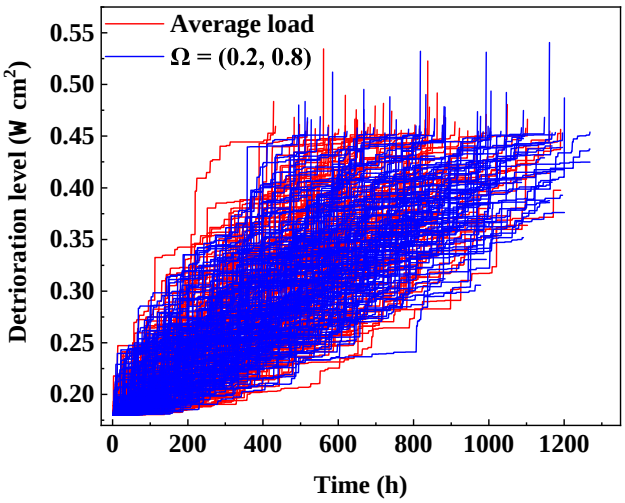

Figure 12. System resistance deterioration trajectories comparison for $L_{demand} = 6.6$ W cm^{-2}.

Conclusion

This work proposed a post-prognostics decision-making strategy for a multi-stack fuel cell system. The system lifetime is managed through the post-decision control of distributing system power demand among stacks. Both fuel cell deterioration and system fuel consumption are considered in the

Table 5. 1500 runs simulation statistic results for $L_{demand} = 6.6$ W cm^{-2}.

Simulations	$\overline{EoL}$	EoL_{med}	$\overline{Ratio}$	$Ratio_{med}$
Daisy chain	759	760	26.3925	26.3925
Average load	774	768	26.5065	26.5065
$\Omega = (0.5, 0.5)$	785	784	25.8183	25.8322
$\Omega = (0.2, 0.8)$	800	804	23.7155	23.8972

management strategy. Fuel cell stack resistance is chosen as a health index and modeled through a stochastic Gamma process. A deterioration function is then built to access system deterioration during operation, together with fuel consumption function. Then, a MOO problem is formulated to take the post-prognostic decisions. The simulation results are obtained and analyzed through a 1500-run simulation on a 3-stack fuel cell system. The simulation results of our approach are compared with the results of the Daisy chain and average load to validate the control efficiency. The main conclusions of this work include:

1) The stochastic gamma process is a relevant tool for modeling fuel cell resistance deterioration. The shape and scale parameters can be estimated from a real-life experiment dataset.
2) MOO proves to be an efficient approach for building a decision-making strategy. A trade-off for conflicting objectives, that are system deterioration and fuel consumption, can be handled through a weighted vector.
3) The proposed approach has been applied for two typical load demands and compared with Daisy chain and average load strategies.
4) For the high power load demand case, the proposed decision-making strategy can help to extend the system lifetime by 25% compared with the Daisy chain strategy.

The next step will be to extend the method to varying power loads. In a broader perspective, improvement work will be to extend the results to more than three stacks. The influence of the number of stacks on control effects will be studied to obtain an optimal system configuration. Implementation in a real case will be also considered. From the methodology point of view, Reinforcement Learning (RL)-based energy management will be considered. RL is suitable to solve sequential decision-making problem, either in model-based or model-free manner. Moreover, the recently developed deep reinforcement learning techniques leverage the powerful representation advantage of neural network, which makes RL a promising technique in various applications, including the energy management of fuel cell systems.

Declaration of Conflicting interests

The authors declare that they have no known competing financial interests or personal relationships that could be appeared to influence the work reported in this paper.

Funding

This work has been partially supported by the the ANR project ANR-15-IDEX-02 and MIAI@Grenoble Alpes (ANR-19-P3IA-0003)

References

1. Council of the European Union. European Green Deal. https://www.consilium.europa.eu/en/policies/green-deal/, 2019. Last accessed on 2022-02-15.
2. Borup RL, Kusoglu A, Neyerlin KC et al. Recent developments in catalyst-related pem fuel cell durability. *Current Opinion in Electrochemistry* 2020; 21: 192–200.
3. Wang Y, Seo B, Wang B et al. Fundamentals, materials, and machine learning of polymer electrolyte membrane fuel cell technology. *Energy and AI* 2020; : 100014.
4. Jouin M, Gouriveau R, Hissel D et al. Prognostics and health management of PEMFC–state of the art and remaining challenges. *International Journal of Hydrogen Energy* 2013; 38(35): 15307–15317.
5. Yue M, Al Masry Z, Jemei S et al. An online prognostics-based health management strategy for fuel cell hybrid electric vehicles. *International Journal of Hydrogen Energy* 2021; 46(24): 13206–13218.
6. Hua Z, Zheng Z, Pahon E et al. Lifespan prediction for proton exchange membrane fuel cells based on wavelet transform and echo state network. *IEEE Transactions on Transportation Electrification* 2021; .
7. Atamuradov V, Medjaher K, Dersin P et al. Prognostics and health management for maintenance practitioners-review, implementation and tools evaluation. *International Journal of Prognostics and Health Management* 2017; 8(060): 1–31.
8. Li Q, Wang T, Dai C et al. Power management strategy based on adaptive droop control for a fuel cell-battery-supercapacitor hybrid tramway. *IEEE Transactions on Vehicular Technology* 2017; 67(7): 5658–5670.
9. Wu X, Hu X, Yin X et al. Convex programming energy management and components sizing of a plug-in fuel cell urban logistics vehicle. *Journal of Power Sources* 2019; 423: 358–366.
10. Yue M, Jemei S, Gouriveau R et al. Review on health-conscious energy management strategies for fuel cell hybrid electric vehicles: Degradation models and strategies. *International Journal of Hydrogen Energy* 2019; 44(13): 6844–6861.
11. Yue M, Jemei S and Zerhouni N. Health-conscious energy management for fuel cell hybrid electric vehicles based on prognostics-enabled decision-making. *IEEE Transactions on Vehicular Technology* 2019; 68(12): 11483–11491.
12. Marx N, Boulon L, Gustin F et al. A review of multi-stack and modular fuel cell systems: Interests, application areas and on-going research activities. *International Journal of Hydrogen Energy* 2014; 39(23): 12101–12111.
13. Liu J and Zio E. Prognostics of a multistack pemfc system with multiagent modeling. *Energy Science & Engineering* 2019; 7(1): 76–87.
14. Marx N, Cárdenas DCT, Boulon L et al. Degraded mode operation of multi-stack fuel cell systems. *IET Electrical Systems in Transportation* 2016; 6(1): 3–11.
15. Calderón AJ, Vivas FJ, Segura F et al. Integration of a multi-stack fuel cell system in microgrids: A solution based on model predictive control. *Energies* 2020; 13(18): 4924.
16. Wang T, Li Q, Yin L et al. Hydrogen consumption minimization method based on the online identification for multi-stack pemfcs system. *International Journal of Hydrogen Energy* 2019; 44(11): 5074–5081.
17. Yan Y, Li Q, Chen W et al. Online control & power coordination method for multi-stack fuel cells system based on optimal power allocation. *IEEE Transactions on Industrial Electronics* 2020; .
18. Herr N, Nicod JM, Varnier C et al. Decision process to manage useful life of multi-stacks fuel cell systems under service constraint. *Renewable energy* 2017; 105: 590–600.
19. Zhou S, Zhang G, Fan L et al. Scenario-oriented stacks allocation optimization for multi-stack fuel cell systems. *Applied Energy* 2022; 308: 118328.

20. Liu Y, Li J, Chen Z et al. Research on a multi-objective hierarchical prediction energy management strategy for range extended fuel cell vehicles. *Journal of Power Sources* 2019; 429: 55–66.
21. Konak A, Coit DW and Smith AE. Multi-objective optimization using genetic algorithms: A tutorial. *Reliability engineering & system safety* 2006; 91(9): 992–1007.
22. Li H, Xu B, Lu G et al. Multi-objective optimization of pem fuel cell by coupled significant variables recognition, surrogate models and a multi-objective genetic algorithm. *Energy Conversion and Management* 2021; 236: 114063.
23. Kim J, Lee SM, Srinivasan S et al. Modeling of proton exchange membrane fuel cell performance with an empirical equation. *Journal of the electrochemical society* 1995; 142(8): 2670.
24. Gouriveau R, Hilairet M, Hissel D et al. Ieee phm 2014 data challenge: Outline, experiments, scoring of results, winners. In *Proc. IEEE Conf. Prognostics Health Manage.* pp. 1–6.
25. Liu H, Chen J, Hissel D et al. Prognostics methods and degradation indexes of proton exchange membrane fuel cells: A review. *Renewable and Sustainable Energy Reviews* 2020; 123: 109721.
26. Bressel M, Hilairet M, Hissel D et al. Extended kalman filter for prognostic of proton exchange membrane fuel cell. *Applied Energy* 2016; 164: 220–227.
27. Liu D, Lin R, Feng B et al. Investigation of the effect of cathode stoichiometry of proton exchange membrane fuel cell using localized electrochemical impedance spectroscopy based on print circuit board. *International Journal of Hydrogen Energy* 2019; 44(14): 7564–7573.
28. Chen F and Gao Y. An algorithm for on-line measurement of the internal resistance of proton exchange membrane fuel cell. *Fuel Cells* 2015; 15(2): 337–343.
29. Ma T, Zhang Z, Lin W et al. Impedance prediction model based on convolutional neural networks methodology for proton exchange membrane fuel cell. *International Journal of Hydrogen Energy* 2021; .
30. Zaccaria V, Tucker D and Traverso A. A distributed real-time model of degradation in a solid oxide fuel cell, part i: Model characterization. *Journal of Power Sources* 2016; 311: 175–181.
31. Laguna-Bercero M, Campana R, Larrea A et al. Electrolyte degradation in anode supported microtubular yttria stabilized zirconia-based solid oxide steam electrolysis cells at high voltages of operation. *Journal of Power Sources* 2011; 196(21): 8942–8947.
32. Takao S, Sekizawa O, Samjeské G et al. Observation of degradation of pt and carbon support in polymer electrolyte fuel cell using combined nano-x-ray absorption fine structure and transmission electron microscopy techniques. *ACS applied materials & interfaces* 2018; 10(33): 27734–27744.
33. Pei P, Chang Q and Tang T. A quick evaluating method for automotive fuel cell lifetime. *International Journal of Hydrogen Energy* 2008; 33(14): 3829–3836.
34. Chen H, Pei P and Song M. Lifetime prediction and the economic lifetime of proton exchange membrane fuel cells. *Applied Energy* 2015; 142: 154–163.
35. Yang S, Choi S, Kim Y et al. Improvement of fuel cell durability performance by avoiding high voltage. *International Journal of Automotive Technology* 2019; 20(6): 1113–1121.
36. Sharaf OZ and Orhan MF. An overview of fuel cell technology: Fundamentals and applications. *Renewable and sustainable energy reviews* 2014; 32: 810–853.
37. Depature C, Jemei S, Boulon L et al. Ieee vts motor vehicles challenge 2017-energy management of a fuel cell/battery vehicle. In *2016 IEEE Vehicle Power and Propulsion Conference (VPPC)*. IEEE, pp. 1–6.
38. van Noortwijk JM. A survey of the application of gamma processes in maintenance. *Reliability Engineering & System Safety* 2009; 94(1): 2–21.

39. Flammia D, Guarino A, Petrone G et al. Enhanced kalman filter-based identification of a fuel cell circuit model in impedance spectroscopy tests. In *ELECTRIMACS 2019*. Springer, 2020. pp. 117–128.
40. Zuo J, Cadet C, Li Z et al. Post-prognostics decision making for a two-stacks fuel cell system based on a load-dependent deterioration model. In *European Conference of the Prognostics and Health management (PHM) Society*, volume 5. p. 9.
41. Deb K, Pratap A, Agarwal S et al. A fast and elitist multiobjective genetic algorithm: Nsga-ii. *IEEE transactions on evolutionary computation* 2002; 6(2): 182–197.
42. Wierzbicki AP. The use of reference objectives in multiobjective optimization. In *Multiple criteria decision making theory and application*. Springer, 1980. pp. 468–486.
43. Blank J and Deb K. Pymoo: Multi-objective optimization in python. *IEEE Access* 2020; 8: 89497–89509.
44. Blank J, Deb K and Roy PC. Investigating the normalization procedure of nsga-iii. In *International Conference on Evolutionary Multi-Criterion Optimization*. Springer, pp. 229–240.
45. Cinlar E, Bažant ZP and Osman E. Stochastic process for extrapolating concrete creep. *Journal of the Engineering Mechanics Division* 1977; 103(6): 1069–1088.
46. Blank J and Deb K. A running performance metric and termination criterion for evaluating evolutionary multi- and many-objective optimization algorithms. In *2020 IEEE Congress on Evolutionary Computation (CEC)*. IEEE, pp. 1–8.

Appendix

Gamma process - scale and shape parameters estimation

The identification of the scale and shape parameters of the gamma process, representing the deterioration modeling are based on the IEEE PHM 2014 data challenge, which provides two typical durability test datasets on two fuel cell stacks[24]. These fuel cell stacks consist of 5 single cells with an active area of 100 cm^2.

The resistance values were fitted based on the measured polarization curves with the aging data, as shown in Fig. 13. The parameters are estimated by using the non-linear least square approach to fit the polarization equation to all measured polarization curves.

The resistance estimations as shown in Fig. (13) are used to estimate the shape and the scale parameters (α and β) of the stochastic deterioration gamma process (section Deterioration and failure behavior modeling). To that aim, the Method of moments (MoM) is applied[45]. From the data, the resistance and time increments are defined as:

$$\begin{aligned} \Delta t_i &= t_i - t_{i-1}, \\ \Delta R_i &= R_i - R_{i-1} \end{aligned} \tag{25}$$

where $i = 1, 2, \cdots n$; n is the number of data.

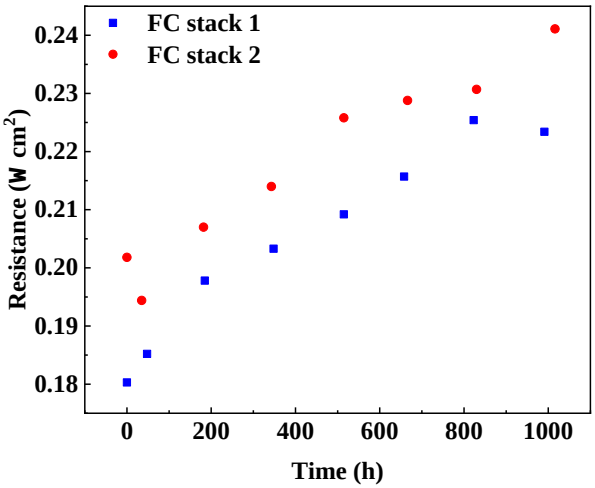

Figure 13. Overall resistance estimated from measured polarization curves, see Fig. 2.

According to Cinlar et al.[45], the estimated values of α and β, written α_0 and β_0, can be determined from the solution of the equations:

$$\begin{aligned} \alpha_0\beta_0 &= \frac{\sum_{i=1}^{n}\Delta R_i}{\sum_{i=1}^{n}\Delta t_i} = \frac{R_n - R_1}{t_n - t_1} \\ R_n\beta_0\left(1 - \frac{\sum_{i=1}^{n}\Delta t_i^2}{\left[\sum_{i=1}^{n}\Delta t_i\right]^2}\right) &= \sum_{i=1}^{n}\left(\Delta R_i - \frac{\Delta t_i (R_n - R_1)}{t_n - t_1}\right)^2 \end{aligned} \tag{26}$$

The estimated parameter values for both FC stack 1 and FC stack 2 are: $\alpha_0 = 0.0075$ and $\beta_0 = 1/27.5$. However, since the values of these parameters are directly linked to the variance of the simulated trajectories, it must be checked that these values are suitable for this application. Indeed, the variance of the trajectories has to be neither too large, because the lifetime would not be controllable, nor too small, because the system would not be stochastic. The trajectories obtained with the estimated values are shown in Fig. 14, and it can been seen that the variance is too high. As the variance of the trajectories is linked with the the scale parameter β, new simulations are carried out with smaller β values ($\beta_0/1.5$ and $\beta_0/3$). To keep the average deterioration level the same, the shape parameter α is also multiplied with the same constant values. The trajectory results in Fig. 14 show that the variance is too small for the value divided by 3. Thus, the proper values are:

$$\begin{aligned} \beta &= \beta_0/1.5 \\ \alpha &= 1.5 \cdot \alpha_0 \end{aligned} \tag{27}$$

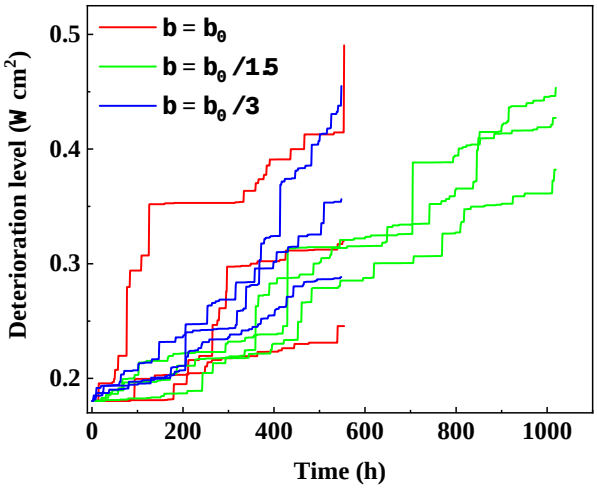

Figure 14. Deterioration trajectories with different scale parameters.

Calculation steps of NSGA-II algorithm

Originally inspired by nature selection, the NSGA-II algorithm can be summarised by the following steps:

(1) Generate the initial population of individuals randomly.
(2) Evaluate the fitness of each individual generated in the population.
(3) Repeat the following operations until the termination condition is satisfied.

   a) Select the best-fit individuals for reproduction;
   b) Create new individuals through selection, crossover, and mutation operations;
   c) Reevaluate the individual fitness of new individuals, replace least-fit population with new individuals.

As depicted in Fig. 15, the algorithm skeleton of NSGA-II stems from classic Genetic algorithm (GA). NSGA-II proposed a modified version of mating and survival selection. A non-dominated sorting and crowding distance are used to determine fitness of individuals, the individuals with better fitness should be retained after selection. Fig. 15 actually describes the t-th generation of NSGA-II. First, a hybrid population of parent population P_t and offspring population Q_t is formed. Then, the population of R_t is sorted according to non-domination, with a size of $2N$. During the the selection process, the elitism is ensured. F_1 collects the solutions of best non-dominated set, emphasized as the best solution. Keep filling the parent population P_{t+1} with sorted best solutions until it reaches population size N. During this process, the crowding distance of non-dominated set F is calculated as criterion to select the best solutions for P_{t+1}. The newly selected parent population P_{t+1} is used to create a new population Q_{t+1} through selection, crossover, and mutation operations. The optimization procedure is stopped when the termination condition is satisfied.

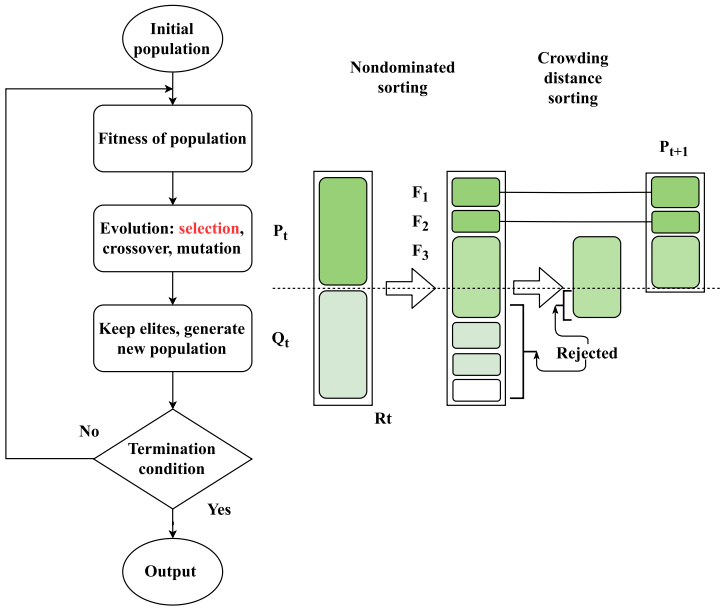

Figure 15. Schematic diagram of NSGA-II.

Convergence of NSGA-II algorithm

The convergence of the NSGA-II algorithm is analyzed for the designed parameters. A newly proposed running performance metric based on the calculation of Inverted Generational Distance (IGD) is used to estimate the convergence of the NSGA-II algorithm[43,46]. This running metric shows the difference in the objective space from the initial generation to the current generation. It is suitable for analyzing the optimization process when the true Pareto Front is not known. This running metric is calculated by accumulating the non-dominated (ND) solutions from initial generation to generation (x):

$$\begin{aligned}\Delta f^x &= IGD(\bar{P}^x(t), \bar{P}^x(x)) \\ &= \frac{1}{|\bar{P}^x(x)|} \sum_{i=1}^{|\bar{P}^x(x)|} \left(\min_{j=1}^{|\bar{P}^x(t)|} \|\bar{P}_i^x(x) - \bar{P}_j^x(t)\| \right)\end{aligned} \tag{28}$$

where x is the accumulated current generation number (here x increment interval is set as 10); $\bar{P}^x(t)$ is the evolving ND set ($0 \leq t \leq x$) and $\bar{P}^x(x)$ is the ND set of current generation x (normalized). This metric is computed for all past generations.

Figure 16 shows the running metric accumulated by a generation step of 10 during one optimization ($L_{demand} = 7.8$ W cm^{-2}, $R_{1,obs} = 0.1903$, $R_{2,obs} = 0.3103$, $R_{3,obs} = 0.2403$ Ω cm^2). A bigger drop in Δf means better improvement for ND solutions. Figure 16(a) shows the algorithm gradually improves for past 60 generation. From Figure 16(c), it can be seen that the algorithm terminates at the 170-th

generation and the Pareto fronts and final decision are plotted in Fig. 16(d) (the black marked point). The final decisions for weight vector $\Omega = (0.2, 0.8)$ are $(L_1, L_2, L_3) = (2.749, 2.430, 2.621)$ W cm^{-2}.

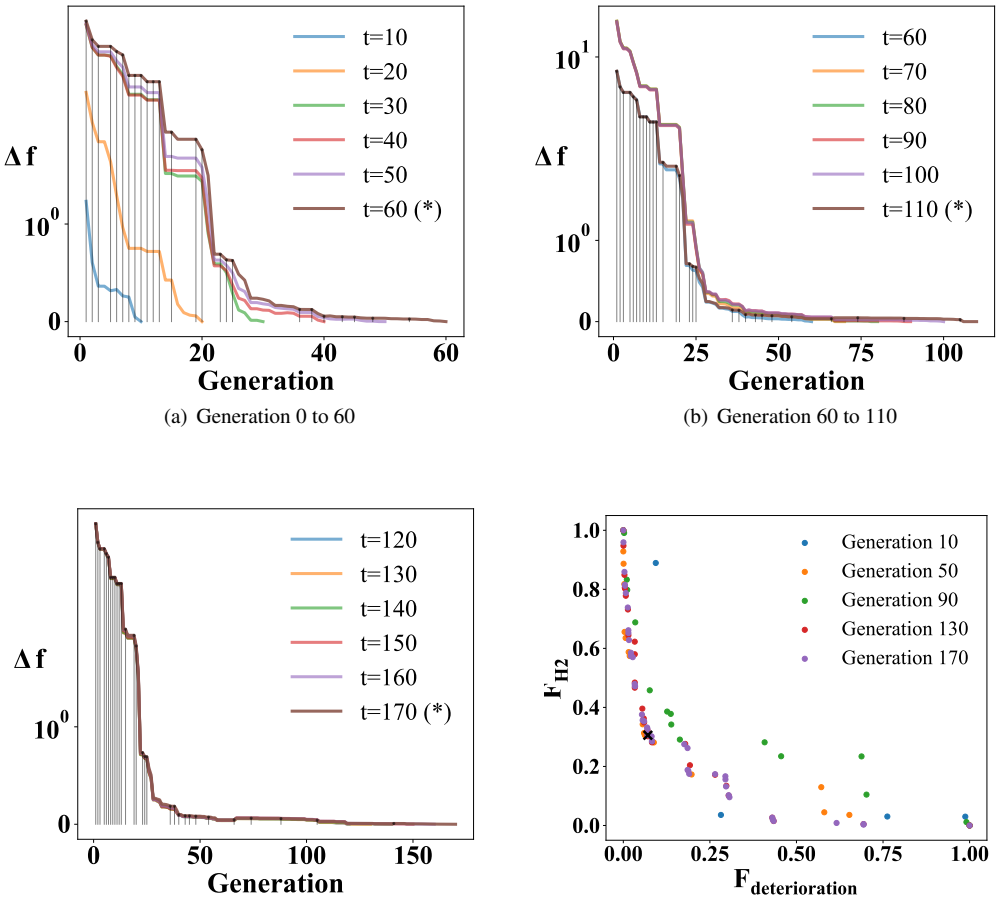

(a) Generation 0 to 60

(b) Generation 60 to 110

(c) Generation 170 to 220

(d) Pareto Front and final decision

Figure 16. Convergence of NSGA-II algorithm.